ELSEVIER

Coastal Engineering 41 (2000) 467–496

COASTAL ENGINEERING

www.elsevier.com/locate/coastaleng

Nonlinear and 3D effects in leaky infragravity waves

A.R. Van Dongeren [a,*], I.A. Svendsen [b]

[a] *Section of Fluid Mechanics, Department of Civil Engineering, Delft University of Technology, Stevinweg 1, 2628 CN Delft, Netherlands*

[b] *Center for Applied Coastal Research, Ocean Engineering Lab, University of Delaware, Newark, DE 19716, USA*

Received 14 August 1999; received in revised form 14 March 2000; accepted 21 March 2000

Abstract

In this paper, infragravity (IG) waves, forced by normally and obliquely incident wave groups, are studied using the quasi-3D (Q3D) nearshore circulation model SHORECIRC [Van Dongeren, A.R., I.A. Svendsen, 1997b. Quasi 3-D modeling of nearshore hydrodynamics. Research report CACR-97-04. Center for Applied Coastal Research, University of Delaware, Newark, 243 pp.], which includes the Q3D effects. The governing equations that form the basis of the model, as well as the numerical model and the boundary conditions, are described. The model is applied to the case of leaky IG waves. It is shown that the Q3D terms have a significant effect on the cross-shore variation of the surface elevation envelope, especially around the breakpoint and in the inner surf zone. The effect of wave groupiness on the temporal and spatial variation of all Q3D terms is shown after which their contribution to the momentum equations is analyzed. This reveals that only those Q3D coefficients, which appear in combination with the largest horizontal velocity shears make a significant contribution to the momentum equations. As a result of the calculation of the Q3D coefficients, the IG wave velocity profiles can be determined. This shows that in the surf zone, the velocity profiles exhibit a large curvature and time variation in the cross-shore direction, and a small — but essential — depth variation in the longshore direction.

Keywords: Infragravity waves; Long waves; Numerical modelling; Surfbeat; Nearshore circulation; Three-dimensional modelling

* Corresponding author. Department MCI, WL|Delft Hydraulics, PO Box 177, 2600 MH Delft, The Netherlands. Fax: +31-15-285-8712.

E-mail addresses: ap.vandongeren@wldelft.nl (A.R. Van Dongeren), ias@coastal.udel.edu (I.A. Svendsen).

0378-3839/00/$ - see front matter
PII: S0378-3839(00)00041-7

1. Introduction

In this paper, we apply the SHORECIRC model to the case of leaky infragravity (IG) waves. SHORECIRC is a quasi-3D (Q3D) nearshore circulation model, which combines the effect of the vertical structure of the IG wave particle velocity profile with a numerical two-dimensional horizontal (2DH) circulation model.

2DH models have been developed to study phenomena, such as the current circulation over periodically longshore-varying bottom topographies Noda et al., 1974; Ebersole and Dalrymple, 1980 and others) and in closed basins with in principle arbitrary bathymetries (Wu and Liu, 1985; Wind and Vreugdenhil, 1986). These models describe the depth-mean current velocity and surface elevation and are based on the depth-averaged and time-averaged Reynolds equations. Since time averaging is done over the short-wave period, the effect of the short-wave motion is replaced by the radiation stress and the short-wave-induced volume flux, which force the long-wave and current motion. These quantities cannot be determined from the wave-averaged equations themselves and have to be supplied to the model through a so-called "short-wave driver". The bottom boundary layer effect is replaced by a wave-averaged bottom shear stress, which in itself is modelled as a function of the depth-averaged velocity. The turbulent shear stresses are represented by an eddy viscosity model, which closes the equations.

These models, however, do not account for the vertical variation of the current or long-wave velocity profiles over depth. Therefore, Q3D models were developed. In an approach by De Vriend and Stive (1987) and Stive and De Vriend (1987), the current is split into primary and secondary flow profiles where the absolute magnitude of the primary velocity vector is assumed to dominate the secondary flow magnitude. This assumption is not valid in the case of normally incident waves. In a different approach, Svendsen and Lorenz (1989) determined analytical expressions for the vertically varying longshore and cross-shore currents separately for the special case of a long straight coast. Svendsen and Putrevu (1990) formulated the steady-state version of the SHORECIRC Q3D nearshore circulation model using analytical solutions for the 3D current profiles in combination with a numerical solution of the depth-integrated 2DH equations for a long straight coast. They split the current velocity into a depth-invariant component and a component with a vertical variation with zero depth-mean flow. Sánchez-Arcilla et al. (1990, 1992) presented a similar concept.

Putrevu and Svendsen (1992) and Svendsen and Putrevu (1994) recognized that the current–current and current–wave interactions neglected in previous investigations induce a nonlinear dispersion mechanism, analogous to the dispersion of solutes (Taylor, 1954; Elder, 1959). This mechanism significantly augments the lateral turbulent mixing and accounts for the difference in magnitude between the vertical and horizontal mixing in the case of a longshore current on a long, straight coast.

The time-dependent version of this model, called SHORECIRC, was presented in Van Dongeren et al. (1994) for the special case of longshore uniformity in both the bathymetric and hydrodynamical conditions. The generalized Q3D governing equations were derived in Putrevu and Svendsen (1997, 1999), and analytical expressions for the velocity profiles were given in Van Dongeren and Svendsen (1997b).

The development of IG waves on a plane slope has been studied earlier using the linearized, depth-averaged equations of motion. Symonds et al. (1982) and Schäffer and Svendsen (1988) analyzed the 1D-horizontal generation of surf beat using different assumptions about the way breaking modifies the wave groupiness. These investigations certified that forcing of IG waves occurs both due to a varying breakpoint and throughout the surf zone due to the changes in wave heights and groupiness in that region. (Schäffer, 1993, 1994) extended this approach to a 2DH study of edge wave generation and generalized the breaking assumption by combining the two extremes considered by Symonds et al. and Schäffer and Svendsen. In all these investigations, the forcing was generated by wave groups formed by a weak modulation of a sinusoidal carrier wave train, which made analytical solutions possible for the steady-state situation that occurs after a long time of periodic forcing. Recently, Lippmann et al. (1997) examined the initial growth rate of such edge waves for the fully resonant case and (Chen and Guza 1998a,b) studied the effect of periodic topographic variations.

In this paper, we will analyze the case of IG waves generated by normally and obliquely incident periodic wave groups using the same forcing as Schäffer (1994), but using the fully nonlinear Q3D SHORECIRC model. This case is a natural extension of the longshore current case studied before, where the restriction of steady, longshore-uniform forcing is replaced by periodic forcing.

First, we will give an outline of the derivation of the Q3D governing equations with an emphasis on the calculation of the depth-varying velocity profiles. Then, we will briefly describe the numerical model and its boundary conditions. The main part of this work is devoted to the analysis of the Q3D terms in the governing equations for the case of leaky IG waves forced by both normally and obliquely incident wave groups. In particular, we will investigate the size of these terms relative to the "conventional" terms that appear in the nonlinear shallow water (NSW) equations. We will also show the effect these terms have on the cross-shore long-wave envelope and show the IG wave velocity profiles.

2. Q3D governing equations

In this section, we will give an overview of the depth-integrated, time-averaged governing equations of the SHORECIRC model. For a more thorough derivation of these equations for the case of depth-uniform currents we refer to the procedure given by Phillips (1977) and Mei (1983), and for the more general case of depth-varying currents to Putrevu and Svendsen (1991, 1997, 1999) and Van Dongeren and Svendsen (1997b).

The conservation of mass equation is given by

$$\frac{\partial \bar{\zeta}}{\partial t} + \frac{\partial}{\partial x_\alpha} \overline{\int_{-h_o}^{\zeta} u_\alpha \mathrm{d}z} = 0 \tag{1}$$

where $\bar{\zeta}$ is the surface elevation of the long (or IG) wave motion, u_α is the total velocity of the long and short waves. The index α represents the horizontal x and y directions.

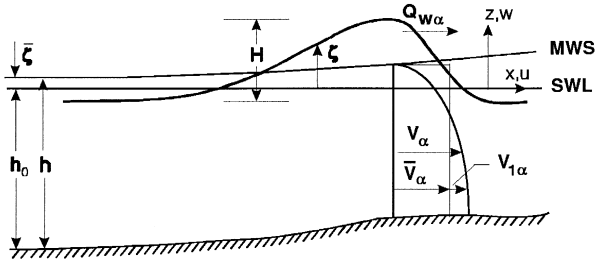

Fig. 1. Definition sketch.

z is the vertical coordinate, defined from the still-water level (SWL) up. h_o is the still-water depth and $h = h_o + \bar{\zeta}$ is the total depth. (See Fig. 1 for a definition sketch.) After turbulence averaging, the total horizontal velocity can be split into a depth-uniform long-wave part $\tilde{V}_\alpha$, a depth-varying long-wave part $V_{1\alpha}$ and a short-wave contribution $u_{w\alpha}$, so that

$$u_\alpha(x,y,z,t) = \tilde{V}_\alpha(x,y,t) + V_{1\alpha}(x,y,z,t) + u_{w\alpha}(x,y,z,t) \tag{2}$$

We define $\overline{u_{w\alpha}} \equiv 0$ below trough level and define the short-wave-induced volume flux above the trough level as

$$Q_{w\alpha} \equiv \overline{\int_{\zeta_t}^{\zeta} u_{w\alpha}\,dz} \tag{3}$$

where ζ_t denotes the trough level of the short-wave motion. The total flux $\bar{Q}_\alpha$ can then be written as

$$\bar{Q}_\alpha \equiv \overline{\int_{-h_o}^{\bar{\zeta}} u_\alpha\,dz} = \tilde{V}_\alpha h + \int_{-h_o}^{\bar{\zeta}} V_{1\alpha}\,dz + Q_{w\alpha} \tag{4}$$

Since the depth-averaged velocity is chosen such that

$$\bar{Q}_\alpha = \tilde{V}_\alpha h \tag{5}$$

we have from Eq. (4) that

$$\int_{-h_o}^{\bar{\zeta}} V_{1\alpha}\,dz = -Q_{w\alpha} \tag{6}$$

With this result, Eq. (1) can be written as

$$\frac{\partial \bar{\zeta}}{\partial t} + \frac{\partial}{\partial x_\alpha}\left(\tilde{V}_\alpha h\right) = 0 \tag{7}$$

The horizontal conservation of momentum can be expressed as

$$\frac{\partial}{\partial t}\left(\tilde{V}_\beta h\right) + \frac{\partial}{\partial x_\alpha}\left(\tilde{V}_\alpha \tilde{V}_\beta h\right) + \frac{\partial}{\partial x_\alpha}\int_{-h_o}^{\bar{\zeta}} V_{1\alpha}V_{1\beta}\,dz + \frac{\partial}{\partial x_\alpha}\overline{\int_{\zeta_t}^{\zeta}\left(u_{w\alpha}V_{1\beta} + u_{w\beta}V_{1\alpha}\right)dz}$$
$$= -g(h_o + \zeta)\frac{\partial \bar{\zeta}}{\partial x_\beta} - \frac{1}{\rho}\frac{\partial}{\partial x_\alpha}\left[S_{\alpha\beta} - \overline{\int_{-h_o}^{\zeta}\tau_{\alpha\beta}\,dz}\right] + \frac{\tau_\beta^S}{\rho} - \frac{\tau_\beta^B}{\rho} \tag{8}$$

where β is index notation for the horizontal x and y directions, $\tau_{\alpha\beta}$ represents the turbulent shear stresses, τ_β^S is the surface stress and τ_β^B is the bottom stress. The radiation stress is defined as[1]

$$S_{\alpha\beta} \equiv \overline{\int_{-h_o}^{\zeta} \left(p\delta_{\alpha\beta} + \rho u_{w\alpha} u_{w\beta} \right) \mathrm{d}z} - \delta_{\alpha\beta} \frac{1}{2} \rho g h^2 \tag{9}$$

The governing equations, Eqs. (7) and (8), are readily solvable numerically in terms of $\overline{Q}_\alpha$ and $\bar{\zeta}$ if the depth variation of the long-wave velocity $V_{1\alpha}$ is known. To determine this would require a full 3D grid and therefore a large computation time. In order to reduce the computational time, we use analytical solutions for the vertical variation of the long-wave current velocity to calculate the integrals in Eqs. (7) and (8). In this way, the integrals can be written in terms of (analytically determined) coefficients multiplied by spatial derivatives of the depth-averaged parameters $\overline{Q}_\alpha$ and $\bar{\zeta}$. In this so-called Q3D approach, only a two-dimensional numerical model is needed.

The mathematics of replacing the depth-dependent terms with depth-invariant coefficients is shown in Appendix A. Substituting the final expression, Eq. (38), from Appendix A into Eq. (8), the Q3D horizontal momentum equations finally become

$$\begin{aligned} &\frac{\partial}{\partial t}\left(\tilde{V}_\beta h\right) + \frac{\partial}{\partial x_\alpha}\left(\tilde{V}_\alpha \tilde{V}_\beta h + M_{\alpha\beta} + A_{\alpha\beta\gamma}\tilde{V}_\gamma\right) \\ &\quad - \frac{\partial}{\partial x_\alpha}\left[h\left(D_{\beta\gamma}\frac{\partial \tilde{V}_\alpha}{\partial x_\gamma} + D_{\alpha\gamma}\frac{\partial \tilde{V}_\beta}{\partial x_\gamma} + B_{\alpha\beta}\frac{\partial \tilde{V}_\gamma}{\partial x_\gamma}\right)\right] \\ &\quad + gh\frac{\partial \bar{\zeta}}{\partial x_\beta} + \frac{1}{\rho}\frac{\partial S_{\alpha\beta}}{\partial x_\alpha} - \frac{\partial}{\partial x_\alpha}\left[h\nu_t\left(\frac{\partial \tilde{V}_\alpha}{\partial x_\beta} + \frac{\partial \tilde{V}_\beta}{\partial x_\alpha}\right)\right] - \frac{\tau_\beta^S - \tau_\beta^B}{\rho} = 0 \end{aligned} \tag{10}$$

Eqs. (7) and (10) are the Q3D equations. They are the generalized version of the equations given in Svendsen and Putrevu (1994) for the special case of steady motion on a cylindrical coast. The dispersive D terms are generalizations of the results found by Taylor (1954) and Fisher (1978). It is important to note here that all the terms in Eq. (10) are functions of either the depth-averaged quantities or the $V_{1\beta}^{(0)}$ velocities, which we can determine from Eq. (30). In this form, the governing equations can readily be coded in a numerical model, which solves the 2DH equations numerically while using the semi-analytical solution of Eq. (30) to represent the effect of the depth-varying currents (or IG waves).

In the remainder of the paper, we will simplify the calculation of the velocity profiles by assuming that they exhibit a quasi-steady response to the forcing. This, in other words, means that the time scale of the motion is sufficiently large so that the acceleration term in Eq. (30) can be neglected. The details are shown in Appendix B.

[1] This definition is symbolically similar to Mei (1983), who uses a different definition of $u_{w\alpha}$, however. He requires $\overline{\int_{-h_o}^{\zeta} u_{w\alpha}\,\mathrm{d}z} = 0$.

3. Numerical solution and boundary conditions

In the version of the SHORECIRC model used here, the governing equations are solved using a central finite difference scheme on a fixed spatial grid with an explicit second-order Adams–Bashforth predictor and a third-order Adams–Moulton corrector time-stepping scheme.

On the artificial, seaward boundary of the computational domain, an absorbing–generating boundary condition is imposed. This boundary condition, which was described in detail in Van Dongeren and Svendsen (1997a), is capable of simultaneously generating incoming and absorbing outgoing waves with a minimum of reflection.

At the landward side of the domain, a shoreline boundary condition based on a simple inundation-drainage procedure is implemented. It is based on a control volume approach in which water is stored in or drained from the shorewardmost wet cell. The procedure is described in detail in Van Dongeren and Svendsen (1997b). On the lateral (shore-normal) boundaries, we use a periodicity condition.

The SHORECIRC model has previously been compared to Visser's (1984) laboratory data of the longshore current profile under monochromatic wave forcing (Svendsen and Putrevu, 1994), to Kostense's (1984) laboratory data of IG waves under normally incident bichromatic wave group forcing (Van Dongeren et al., 1995), and to Haller and Dalrymple's (1999) laboratory data of a rip current system (Haas et al., 1998). In addition, the model has been applied DELILAH (1990) field data of shear wave motions (Svendsen et al., 1997) and to field data of IG wave motions (Van Dongeren et al., 2000). However, the authors know no laboratory data of IG wave motion under obliquely incident bichromatic wave groups to compare the present numerical results to.

4. Application: leaky IG waves

In the following, we will investigate the effect of the Q3D terms on IG waves due to normally and obliquely incident wave groups, but limit the investigation to the case of leaky IG waves.

The wave groups consist of two sinusoidal short-wave components that have a slightly different frequency, but have the same incident direction of propagation at a given depth (Schäffer, 1994). As the obliquely incident wave groups propagate towards shore at the group speed c_g, they refract towards the shore-normal direction whereby it is assumed that both short-wave components refract in the same way and that they do not diverge. The incoming bound IG wave forced by the wave groups propagates with the groups. As the wave groups approach the beach and the short waves are dissipated, this incoming IG wave is modified by the wave group transformation and is released. It will then reflect from the shore and propagate and refract seawards as a free long wave (see Fig. 2 for a definition sketch).

In the following, this process will be illustrated by analyzing the linearized model results and comparing to the linear, analytical solution by Schäffer (1994). Then, we will show the effect that the nonlinear terms in the 2DH shallow water equations have on the solution, and finally we will discuss the relative importance of the Q3D terms.

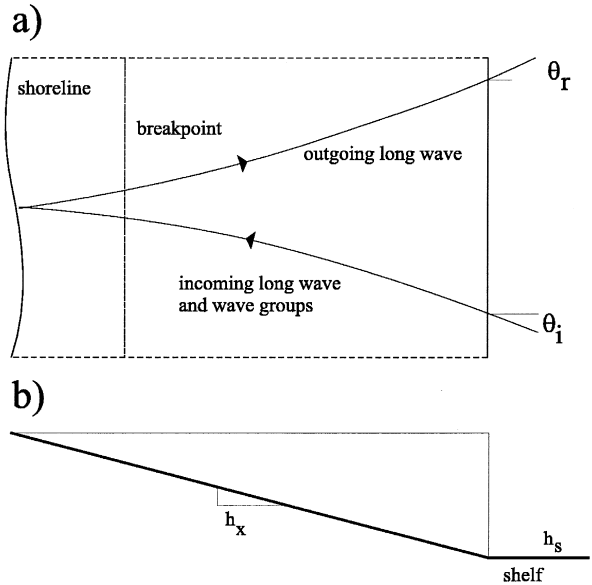

Fig. 2. Definition sketch of obliquely incident and obliquely reflected IG waves.

4.1. Comparison to the linear analytical solution

We first consider the linearized governing equations for the time-varying motion on a plane beach connected to an offshore shelf. For reference, the linearized equations of continuity and momentum solved by Schäffer (1994) read

$$\frac{\partial \bar{\zeta}}{\partial t} + \frac{\partial \overline{Q}_\alpha}{\partial x_\alpha} = 0 \tag{11}$$

$$\frac{\partial \overline{Q}_\beta}{\partial t} + gh_o \frac{\partial \bar{\zeta}}{\partial x_\beta} + \frac{1}{\rho}\frac{\partial S_{\alpha\beta}}{\partial x_\alpha} = 0 \tag{12}$$

We consider the analytical short-wave forcing generated by a wave group consisting of two sinusoidal short waves that have a slightly different frequency but have the same direction of propagation. Given this short-wave forcing, the radiation stress $S_{\alpha\beta}$ can be written as (generalizing from Schäffer, 1994)

$$\begin{aligned} S_{\alpha\beta}(x,y,t) &= \rho g P_{\alpha\beta} H_1^2 (1 + 2\delta\cos(2\vartheta)), \qquad h \geq h_b \\ S_{\alpha\beta}(x,y,t) &= \rho g P_{\alpha\beta} \gamma^2 h_o^2 (1 + 2\delta(1-\kappa)\cos(2\vartheta)), \qquad h \leq h_b \end{aligned} \tag{13}$$

where H_1 is the height of the carrier wave and the wave height modulation $\delta = H_2/H_1$ is the ratio of the wave heights of the secondary wave to the primary wave in the group. In this formulation, it is assumed that δ is small. κ is the breaking location parameter (Schäffer, 1994), where a value of $\kappa = 0$ implies that the breakpoint is in a fixed

location, irrespective of the individual wave height, and that wave groupiness is transmitted into the surf zone according to the Schäffer and Svendsen (1988) model. A value of $\kappa = 1$ implies that the breakpoint is moving on the time scale of the wave groups according to the Symonds et al. (1982) model. In the surf zone, the saturated breaking criterion is $H_1 = \gamma h_o$, and $P_{\alpha\beta}$ is the nondimensional shape parameter for the short waves. Using sine wave theory for the short waves, the shape factor $P_{\alpha\beta}$ in Eq. (13) is defined as

$$P_{\alpha\beta} = \frac{1}{16}\left[\left(1 + \frac{2kh_o}{\sinh 2kh_o}\right)\frac{k_\alpha k_\beta}{k^2} + \frac{2kh_o}{\sinh 2kh_o}\delta_{\alpha\beta}\right] \tag{14}$$

where $k_{\alpha\beta}$ are components of the wave number of the carrier short-wave motion and $\delta_{\alpha\beta}$ is the Kronecker delta.

The phase function is defined following Schäffer (1994), his Eqs. (5) and (6), as

$$2\vartheta = \int_0^x K_x \mathrm{d}x + K_y y - \Delta\omega t \tag{15}$$

The forcing frequency $\Delta\omega$ is the difference frequency between the frequencies ω_1 and ω_2 of the two short waves in the group

$$\Delta\omega \equiv \omega_1 - \omega_2 = 2\epsilon\omega \tag{16}$$

where ϵ is the frequency modulation between the two waves in the wave group and ω is the mean of ω_1 and ω_2. In Eq. (15), K_x and K_y are the x and y components of the wave number of the wave group, or in other words, they are the x and y components of the difference between the wave number components of the two short waves, $k_x^{(1)}$ and $k_x^{(2)}$. After some manipulation, this can be rewritten as

$$K_x \equiv k_x^{(1)} - k_x^{(2)} = 2\epsilon\frac{k}{\cos\theta_i}\left(\frac{1}{n} - \frac{\sin^2\theta_i}{n_s}\right) \tag{17}$$

where $n = c_g/c$ and θ_i is the angle of incidence of the short waves with respect to the normal, and the subscript s denotes conditions on the shelf. We also have

$$K_y \equiv k_y^{(1)} - k_y^{(2)} = 2\epsilon\frac{k\sin\theta_i}{n_s} \tag{18}$$

for the variation in the longshore direction (consistent with Schäffer's (1994) Eq. (8)). The alongshore wave number is constant under Snell's Law for parallel depth contours.

In the model formulation, we have chosen to retain the idea of considering a coastal slope rising from an outer, gentler slope (equivalent to the shelf in Schäffer's (1994) analysis) rather than the plane slope to infinitely large depth recommended by Lippmann et al. (1997). The reasons are the following. On the outer slope, we assume that the depth varies so gently that the waves stay in local equilibrium and that at the toe of the coastal slope, the set-down wave corresponds to the equilibrium bound wave. This avoids the difficulty encountered by, e.g., Lippmann et al. (1997) in justifying the use of long-wave theory in the deepwater part of their plane slope. It also enables us to specify the conditions at the toe as a simple boundary condition for the inflow to the coastal slope. This gives a much more flexible approach than the restricted case of a plane slope

studied by Lippmann et al. (1997). In the present study, we limit the analysis to a plane coastal slope to facilitate a comparison to analytical results, but it should be emphasized that the model can be run on an arbitrary bottom topography.

On the shelf we will assume an equilibrium bound long wave

$$\bar{\zeta}_{\mathrm{i}} = -\frac{1}{\rho}\frac{S_{xx}^{(1)}}{\left(gh_{\mathrm{s}} - c_{\mathrm{gs}}^2\right)} \tag{19}$$

where the subscript s denotes conditions on the shelf and $S_{xx}^{(1)}$ is the time-varying part of Eq. (13), which propagates in the direction of the wave groups. This solution was first found by Longuet-Higgins and Stewart (1962).

In the linearized version of the model, we impose a no-flux condition at the still-water shoreline. At the lateral boundaries, we impose periodicity. The longshore domain length is put equal to the longshore projection of the IG wave length.

In the following case, the frequency modulation is chosen as $\varepsilon = 0.1$, the mean frequency of the short waves is $\omega = 1.8\ \mathrm{s}^{-1}$ and the frequency of the IG wave is $\Delta\omega = 0.36\ \mathrm{s}^{-1}$. The breaking index is $\gamma = 0.75$, and in order to illustrate the effect of the wave groupiness inside the surf zone, we choose first to consider the case of a fixed breaker location by, i.e., $\kappa = 0$ in Eq. (13). The beach slope is chosen as $h_x = 1/20$.

The other input parameters are the shelf depth, h_{s}, the carrier wave frequency ω, the height $H_{1,\mathrm{s}}$ of the carrier wave on the shelf, and the amplitude modulation δ.

This large number of seemingly independent parameters makes this a complicated problem to specify. However, analysis of the problem formulation (Van Dongeren and Svendsen, 1997b) shows that these parameters can be cast into three controlling dimensionless parameters, which read

$$S_{\Delta}^2 = \frac{gh_x^2}{h_{\mathrm{s}}\Delta\omega^2} = 6.31\times10^{-2} \tag{20}$$

$$\frac{h_{\mathrm{b}}}{h_{\mathrm{s}}} = \frac{1}{\gamma}\sqrt{\frac{c_{\mathrm{g,s}}}{c_{\mathrm{g,b}}}}\,\frac{H_{1,\mathrm{s}}}{h_{\mathrm{s}}} = 0.3 \tag{21}$$

$$\kappa = 0 \tag{22}$$

Notice that this is a reduction from the five parameters used by Schäffer (1993). Here, S_{Δ} is equivalent to the slope parameter $S = h_x L/h$ of Svendsen and Hansen (1976) for IG wave motion.

The values chosen above for these parameters imply that the short waves will break at $h_{\mathrm{b}}/h_{\mathrm{s}} = 0.3$. In choosing these parameters, we have also made sure that the incident wave groups travel in intermediate to deep water on the shelf (since $n_{\mathrm{s}} = c_{\mathrm{g}}/c = 0.721$), and that the waves break at a location so that there is a considerable surf zone width. The grid spacings used in the numerical solution are $\Delta x = h_{\mathrm{s}}/3$, $\Delta y = h_{\mathrm{s}}$ and the Courant number $\nu = 0.7$. By comparison with the results for smaller grid sizes, it is found that this grid spacing gives sufficient accuracy all the way to the shoreline.

First, we will consider the special case of normally incident wave groups, which force 2D surfbeat. Fig 3a shows the comparison of the envelopes of the total long-wave

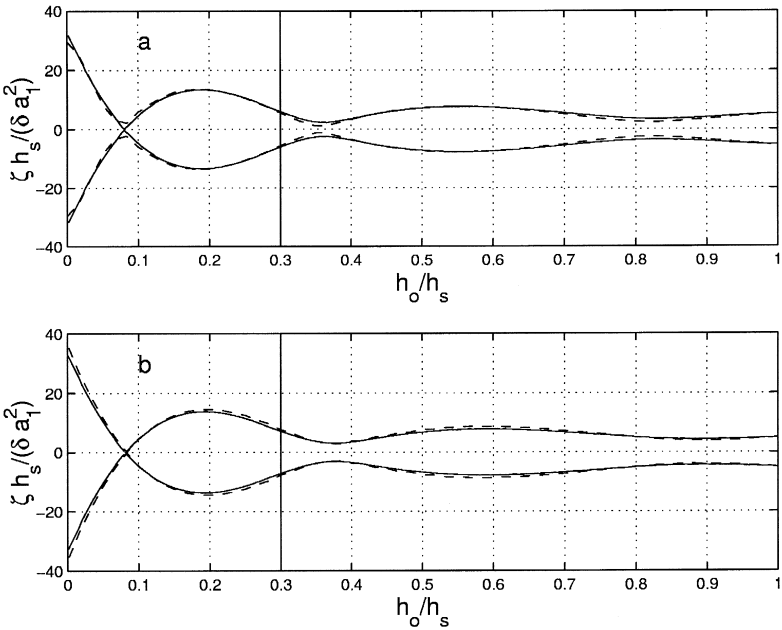

Fig. 3. Envelope of the total long-wave motion vs. depth: present linearized model (solid line) and Schäffer's (1993, 1994) analytical solution (dashed line): (a) normally incident wave groups $\theta_{i,s} = 0°$; (b) obliquely incident wave groups $\theta_{i,s} = 22.37°$. The breakpoint is located at $h_o / h_s = 0.3$.

motion. The solid line indicates the present linearized model and the dashed line indicates the analytical solution by Schäffer and Svendsen (1988) and Schäffer (1993). The agreement is very good, which confirms the accuracy of the numerical computations. The small discrepancies are due to the coarser resolution of the numerical model.

The envelope represents the maximum and minimum surface elevation and is normalized by $\delta a_1^2/h_s$, where $a_1 = H_1/2$. This normalization is chosen such that the incoming bound long wave becomes an $O(1)$ quantity, which can be seen from a scaling analysis of the dimensional Eq. (19)

$$\bar{\zeta}_i = -\frac{1}{\rho}\frac{S_{xx}^{(1)}}{\left(gh_s - c_{gs}^2\right)} = O\left(\frac{\rho g \delta a_1^2}{\rho g h_s}\right) = O\left(\frac{\delta a_1^2}{h_s}\right) \tag{23}$$

where we have used the expression for the time-varying part of the radiation stress in Eq. (13).

The shore normal coordinate is made dimensionless by h_s, so that $h_o/h_s = 0$ corresponds to the still-water shoreline and $h_o/h_s = 1$ to the toe of the slope. The breakpoint is located at $h_o/h_s = 0.3$ in this case.

Fig. 3b shows the comparison between the present model and the analytical solution by Schäffer (1994) for the case of an angle of incidence on the shelf of $\theta_{i,s} = 22.37°$, which corresponds to an alongshore wave length of the IG wave of 150 m. The angle of incidence is less than the limiting angle of incidence $\theta_{i,s}^{max} = 37.07°$, so that the IG wave

motion is "leaky", i.e., the outgoing long waves reach the shelf and are not trapped. The angle of the outgoing long wave on the shelf will then be $\theta_{r,s} = 39.1°$. The agreement is again very good, which confirms the accuracy of the (linear part of the) numerical solution.

4.2. Nonlinear 2DH and Q3D terms

As a next step, we will include in the model the nonlinear terms so that the governing equations correspond to the nonlinear shallow water equations with forcing. At the landward side of the domain, we impose the shoreline boundary condition described in the previous section in order to allow for run-up and run-down.

Fig. 4 shows the envelope of the short-wave-averaged surface elevation (dashed line). Comparing to the linear solution (which is a linear superposition of the steady set-up and the long-wave envelope in Fig. 3(a) and plotted here as the dash-dotted line), we see that including the nonlinear terms shifts the nodes and anti-nodes of the envelopes and changes the amplitudes of the anti-nodes.

If we include the Q3D terms using Eqs. (1) and (10), the cross-shore envelope of the surface elevation changes even more (see Fig. 4, solid line). The Q3D terms have a large effect on the envelope in the surf zone and in the area around the breakpoint, a point that will be discussed in more detail below. The nodes of the envelope, however, do not seem to have shifted significantly relative to the 2DH solution for this particular case.

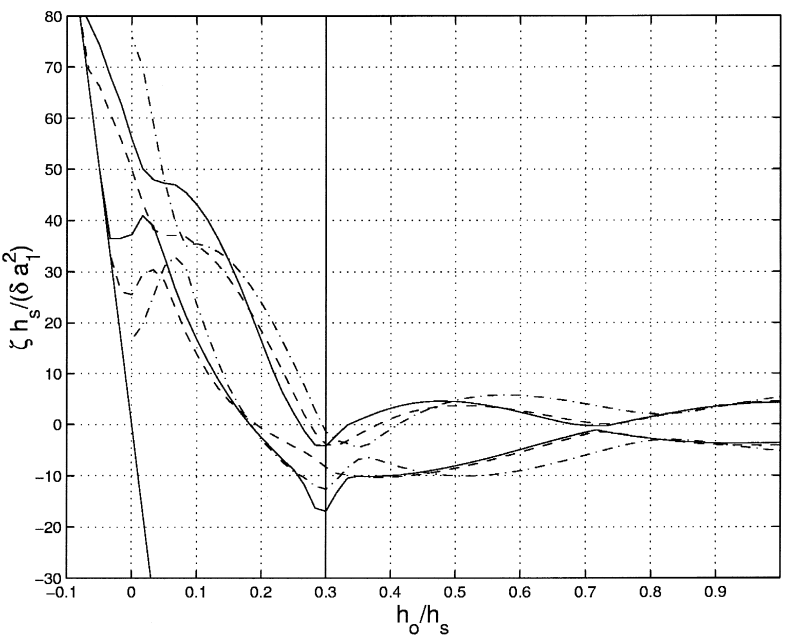

Fig. 4. Envelope of the surface elevation of the IG wave with an angle of incidence of $\theta_{i,s} = 0°$ vs. cross-shore distance: linear analytical solution by Schäffer and Svendsen (1988) (dash-dotted line); SHORECIRC without Q3D terms (dashed line); SHORECIRC with Q3D terms (solid line). The breakpoint is located at $h_o / h_s = 0.3$.

For the case of obliquely incident wave groups, Fig. 5 shows the envelope of the short-wave-averaged surface elevation (dashed line). Again, comparing to the linear solution, the nonlinear terms shift the nodes and anti-nodes in a similar way as was noticeable in the normally incident case. Here also, the Q3D terms have the largest effect on the envelope in the surf zone and particularly in the area around the breakpoint.

Fig. 6 shows a snapshot of the surface elevation at a particular time for the obliquely incident case. To better illustrate the pattern, we have shown three wave lengths in the longshore y direction.

For comparison, Fig. 7 shows the snapshot of the surface elevation at approximately the same time instance in the case when the linearized model with the same input conditions is used.

4.2.1. Time and depth variation of the IG wave particle velocities

In order to calculate the Q3D terms in the momentum equations, we have to determine the vertical variation of the IG wave particle velocities from Eq. (45). It is illustrative to use this numerical output and plot the IG particle velocity profiles at various locations and at various time instances.

Fig. 8 shows the IG particle velocity profiles for three different locations on the slope: ($h_o/h_s = 0.42$, 0.17 and 0.07) and at five time intervals of the IG wave period.

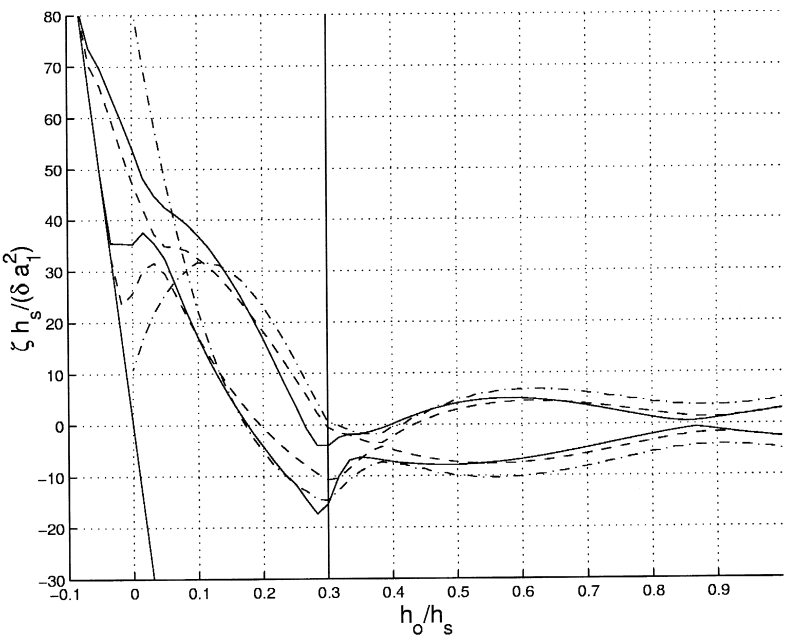

Fig. 5. Envelope of the surface elevation of the IG wave with an angle of incidence of $\theta_{i,s} = 22.37°$ vs. cross-shore distance: linear analytical solution by Schäffer and Svendsen (1988) (dash-dotted line); SHORECIRC without Q3D terms (dashed line); SHORECIRC with Q3D terms (solid line). The breakpoint is located at $h_o / h_s = 0.3$.

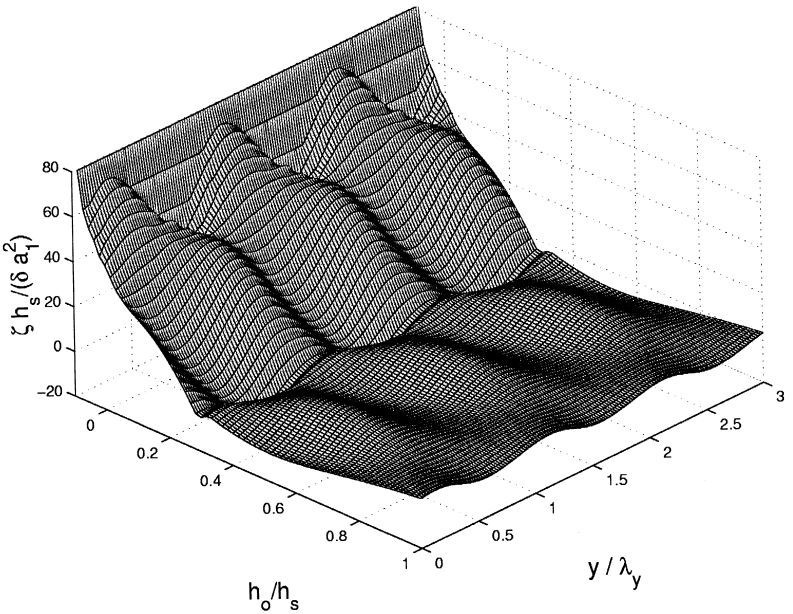

Fig. 6. Snapshot of the surface elevation using the Q3D model.

The motion is a result of the forcing by the obliquely incident wave groups, and of the incoming IG wave and the obliquely reflected IG wave. It is important to notice that the

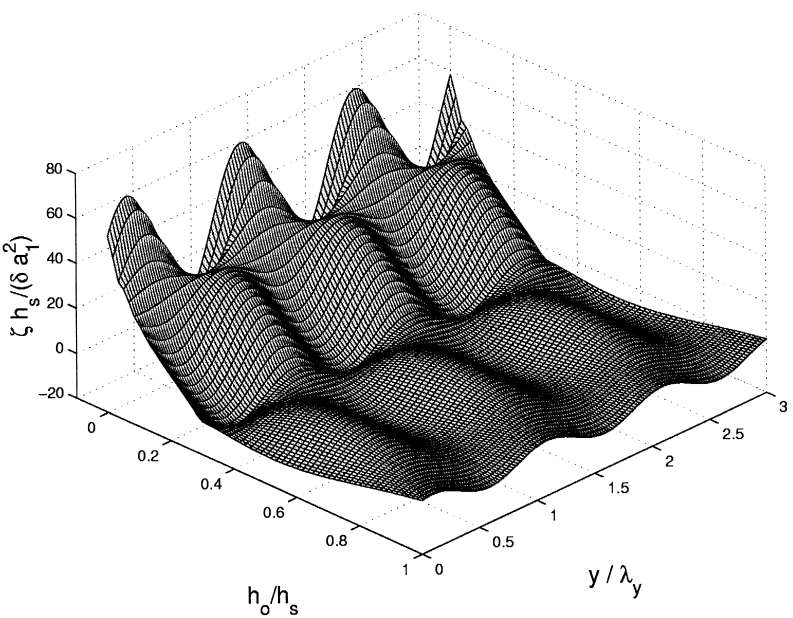

Fig. 7. Snapshot of the surface elevation using the linearized model.

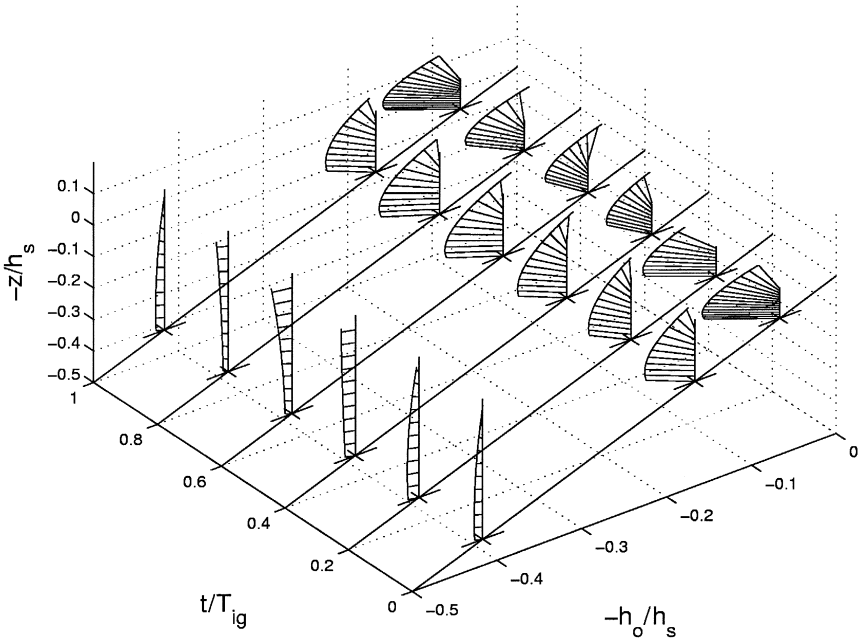

Fig. 8. IG wave profiles for three locations ($h_o / h_s = 0.42$, 0.17 and 0.07) and for five time instances of the IG wave period. The breakpoint is located at $h_o / h_s = 0.3$.

steady part of the short-wave forcing (Eq. (13)) drives a steady longshore current, which is included in the figure, and that the time-varying part of the forcing causes a variation of the velocity profiles over an IG period, so in essence, the picture shown in Fig. 8 corresponds to an IG wave motion riding on top of a relatively strong current.

Since the breakpoint is located at $h_o/h_s = 0.3$, the location $h_o/h_s = 0.42$ is outside the surf zone. The IG wave velocity profiles at that location show a slight curvature in the cross-shore direction and essentially vary linearly with depth in the longshore direction. The two locations inside the surf zone show much more variation. Also, the cross-shore velocity profiles vary significantly over one IG wave period, especially at $h_o/h_s = 0.07$.

The details of the variation of the velocity profiles can better be seen in Fig. 9, which shows the projections of the profiles in the longshore and cross-shore direction. Fig. 9(a) shows the cross-shore velocity (the "undertow") normalized by the local long-wave celerity $c_o = \sqrt{gh_o}$ vs. normalized depth at $h_o/h_s = 0.42$, which is located well outside the surf zone, for 10 intervals per IG wave period. It can be seen that the profiles are slightly curved and, also, that the vertical gradient varies substantially with time. This is due to the (time-varying) forcing f_x in Eq. (45), which is a function of the radiation stress gradients, the pressure gradient and the gradients in the short-wave velocities.

Fig. 9(b) shows the longshore velocity V at the same location outside the surf zone. Due to the relatively small angle of incidence of the short-wave groups, the forcing induced by the short waves in the y direction is also small. This means that these

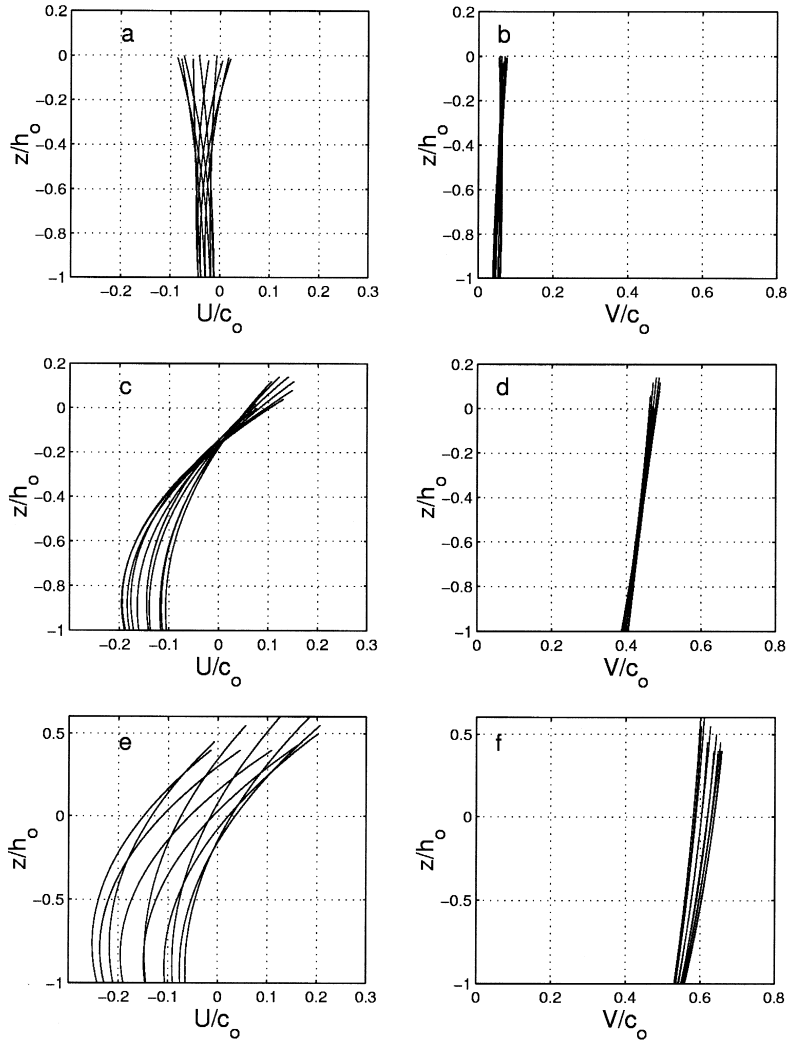

Fig. 9. IG wave particle velocities in the cross-shore and longshore direction normalized by the longwave celerity c_o vs. normalized depth for 10 intervals per IG wave period: (a) Cross-shore velocity U at $h_o / h_s = 0.42$; (b) Longshore velocity V at $h_o / h_s = 0.42$; (c) U at $h_o / h_s = 0.17$; (d) V at $h_o / h_s = 0.17$; (e) U at $h_o / h_s = 0.07$; and (f) V at $h_o / h_s = 0.07$.

profiles are fairly linear with only a slight curvature. The mean over depth is nonzero due to due to the lateral mixing which is mostly dispersive (Svendsen and Putrevu, 1994).

The cross-shore profiles in Fig. 9(c) and (e) exhibit the typical characteristic time-varying undertow profile inside the surf zone that was previously shown by Putrevu and Svendsen (1995) and tested against laboratory data by Smith and Svendsen (1995). The longshore profiles in Fig. 9(d) and (f) are slightly more tilted than the

longshore current profile in Fig. 9(b) because inside the surf zone, a strong mean forcing is present due to the difference between the radiation stress gradient and the pressure gradient. The time variation of the longshore profiles is not very large due to the fact that inside the surf zone the short-wave groups have refracted to near normal incidence.

4.3. Relative magnitude of Q3D coefficients

The relative magnitude of the Q3D coefficients can be calculated directly from the model results under the assumption of quasi-steady state. The analytical approximations used are given in Appendix B as Eqs. (50)–(53).

For the case of normally incident wave groups, Fig. 10 shows the variation in the cross-shore direction of the Q3D coefficients for five time intervals per IG wave period. In the figure, $h_o/h_s = 0$ corresponds to the still-water shoreline and $h_o/h_s = 1$ to the toe of the beach. Although the results are presented in dimensional form, the important feature of this figure is that it gives an indication of the variation of the magnitude of these coefficients. It is also emphasized that the coefficients appear in the equations as coefficients to terms involving the depth-averaged velocity $\tilde{V}_\alpha$ defined by Eq. (5) or the gradients of those velocities. Therefore, the importance of the entire terms in the governing equations will also be discussed below.

In Fig. 10, we have split the M_{xx} term in Eq. (35) into an integral term

$$C_{xx} = \int_{-h_o}^{\bar{\zeta}} U_1^{(0)} U_1^{(0)} \mathrm{d}z \tag{24}$$

and a term for the surface contribution

$$E_{xx} = 2U_1^{(0)}\left(\bar{\zeta}\right) Q_{wx} \tag{25}$$

so that

$$M_{xx} = C_{xx} + E_{xx} \tag{26}$$

In the case of shore-normal flow considered here, all the y components are zero, and coefficients involving y components are not shown. All other coefficients show a large time variation over an IG wave period, especially when compared with the magnitude found for the case of no groupiness ($\delta = 0$), indicated by the thick line. This indicates that even a small temporal and spatial variation in the forcing induces an increased curvature in the velocity profiles, which increases the Q3D terms. This aspect will be discuss in more detail for the case of obliquely incident wave groups. Note that in this and following figures, the magnitude of some of the coefficients increases with the cross-shore coordinate. This is due to the fact that powers of the total depth appear in Eqs. (50)–(53).

For the case of obliquely incident wave groups at an angle of $\theta_{i,s} = 22.37°$, Figs. 11–13 show the variation in the cross-shore direction of these Q3D coefficients for five time intervals per IG wave period. These figures give an indication of the magnitude of these coefficients relative to each other.

Fig. 11 shows that the B and D coefficients exhibit a quite large variation over an IG wave period, which indicates that the local time-varying forcing is very important. It can

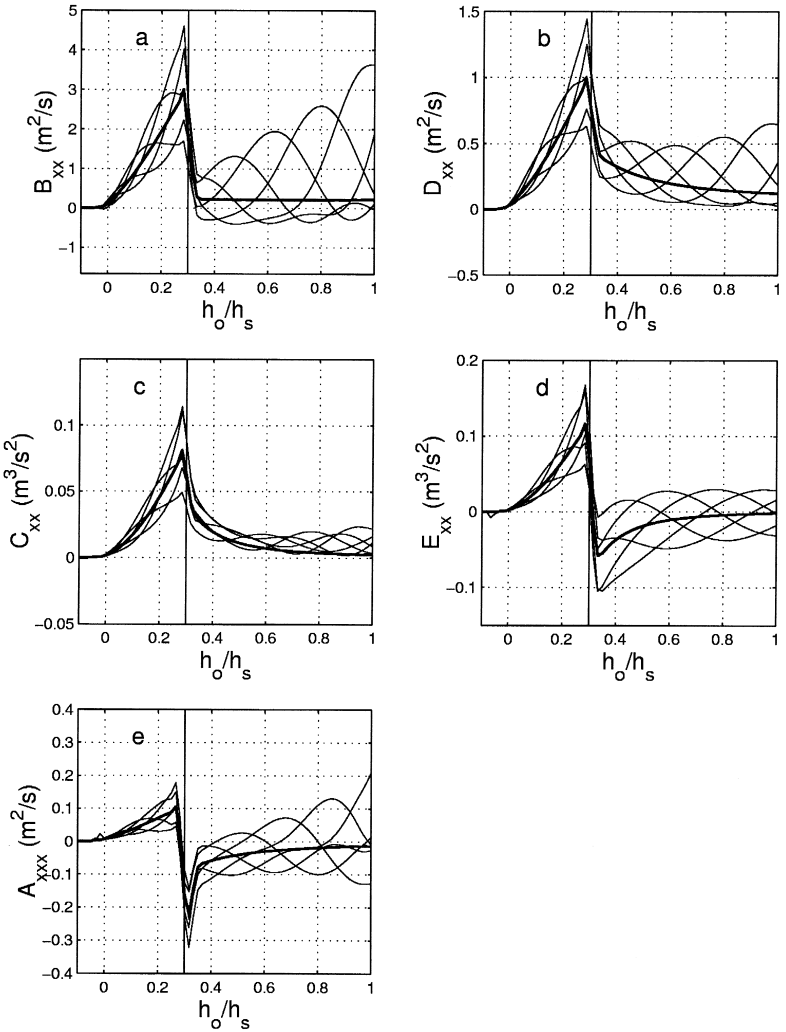

Fig. 10. Magnitude of Q3D coefficients vs. cross-shore distance h_o / h_s for five intervals per IG wave period for the case of $\theta_{i,s} = 0°$: (a) B_{xx}; (b) D_{xx}; (c) C_{xx}; (d) E_{xx}; and (e) A_{xxx}. The case of no groupiness is indicated by the thick solid line. The still-water shoreline is located at $h_o / h_s = 0$ and the breakpoint at $h_o / h_s = 0.3$.

also be seen that the magnitude of all coefficients is significantly larger than the magnitudes, which would have been found for the case of no groupiness ($\delta = 0$), which is indicated by the dashed line. The values increase significantly across the breakpoint, since the "undertow" profiles become much more curved inside the surf zone due to the increased forcing. Because of the simple short-wave modeling, this transition in curvature occurs very rapidly, which increases the cross-shore gradients of the Q3D coefficients. The figure shows that the $B_{\alpha\beta}$ coefficients are in general larger than the

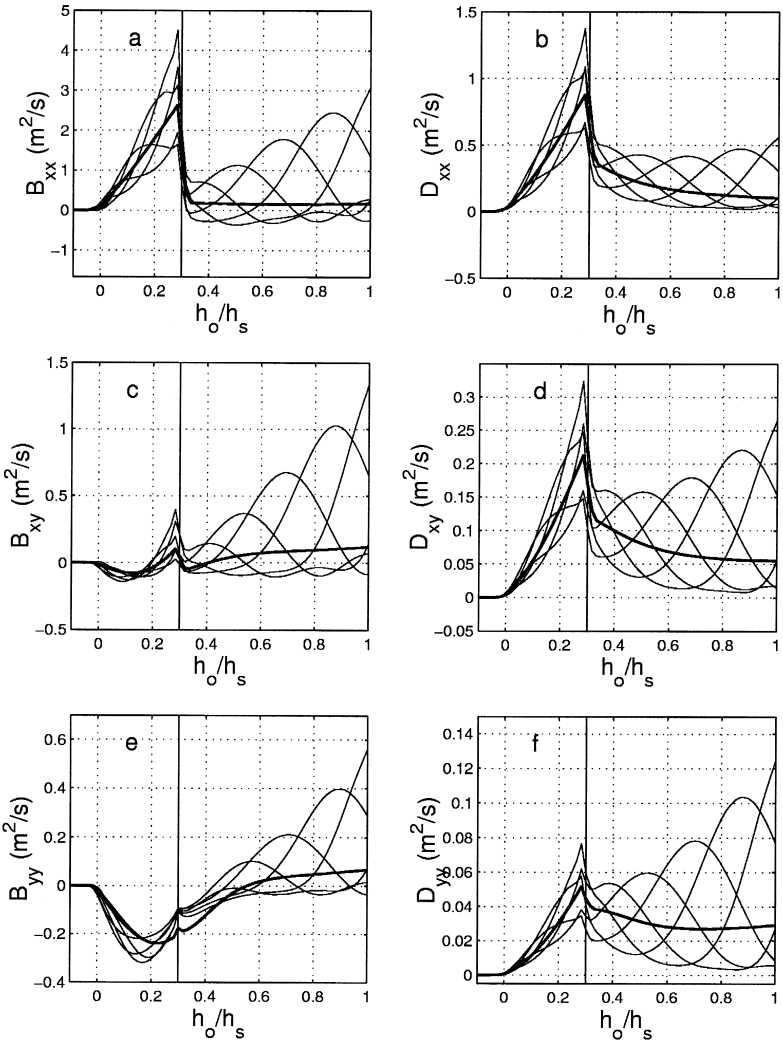

Fig. 11. Magnitude of B and D coefficients vs. cross-shore distance h_o/h_s for five intervals per IG wave period for the case of $\theta_{i,s} = 22.37°$: (a) B_{xx}; (b) D_{xx}; (c) B_{xy}; (d) D_{xy}; (e) B_{yy}; and (f) D_{yy}. The case of no groupiness is indicated by the thick solid line. The still-water shoreline is located at $h_o/h_s = 0$ and the breakpoint at $h_o/h_s = 0.3$.

corresponding $D_{\alpha\beta}$ coefficients, but since these coefficients are multiplied by $(\partial\tilde{V}_\gamma/\partial x_\gamma) \simeq -(\partial W/\partial z)$, which is close to zero, we can expect the $D_{\alpha\beta}$ terms to be more important.

We also see that the D_{xx} and B_{xx} coefficients are larger than the D_{xy} and B_{xy} coefficients, which are in turn larger than the D_{yy} and B_{yy} coefficients. This is because the short-wave groups refract towards the shore-normal, which means that the cross-shore forcing f_x in Eq. (45) becomes dominant over the forcing in the longshore direction. Eq.

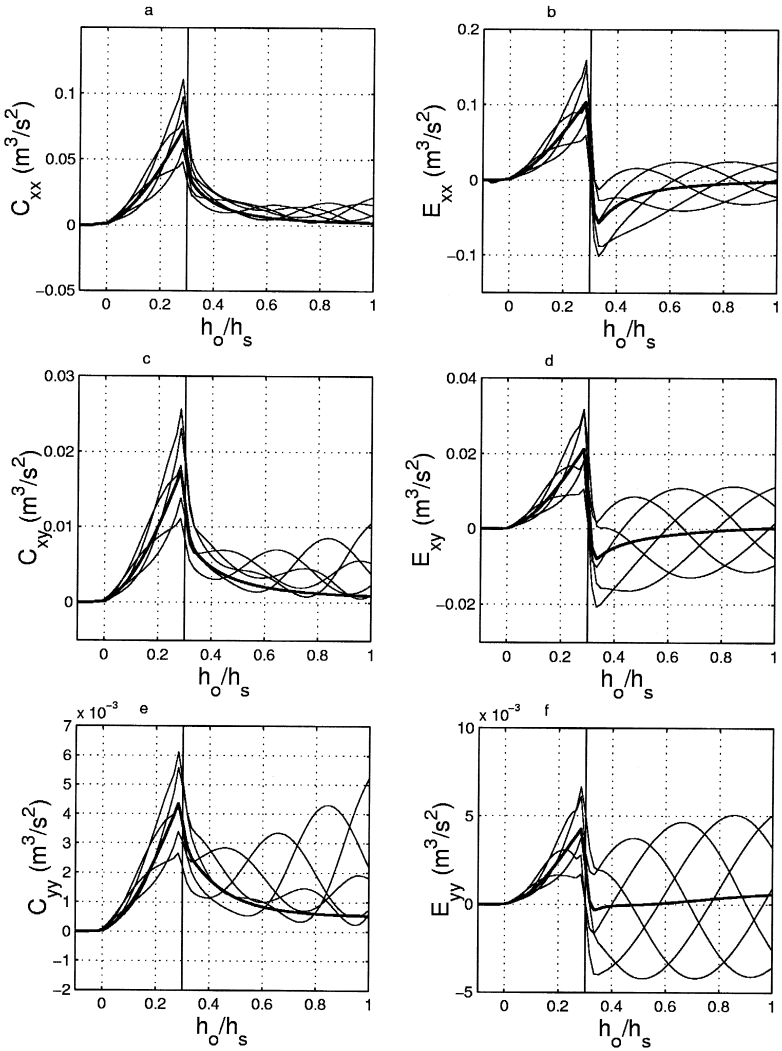

Fig. 12. Magnitude of C and E coefficients vs. cross-shore distance h_o/h_s for five intervals per IG wave period for the case of $\theta_{i,s} = 22.37°$: (a) C_{xx}; (b) E_{xx}; (c) C_{xy}; (d) E_{xy}; (e) C_{yy}; and (f) E_{yy}. The case of no groupiness is indicated by the thick solid line. The still-water shoreline is located at $h_o/h_s = 0$ and the breakpoint at $h_o/h_s = 0.3$.

(45) also implies that the cross-shore velocities are more curved than the longshore velocities, which could already be seen in Fig. 9. This curvature of the velocity profiles directly influences the magnitude of the dispersive coefficients.

For convenience, we will again split the $M_{\alpha\beta}$ term in Eq. (35) into an integral term

$$C_{\alpha\beta} = \int_{-h_o}^{\bar{\zeta}} V_{1\alpha}^{(0)} V_{1\beta}^{(0)} \mathrm{d}z \tag{27}$$

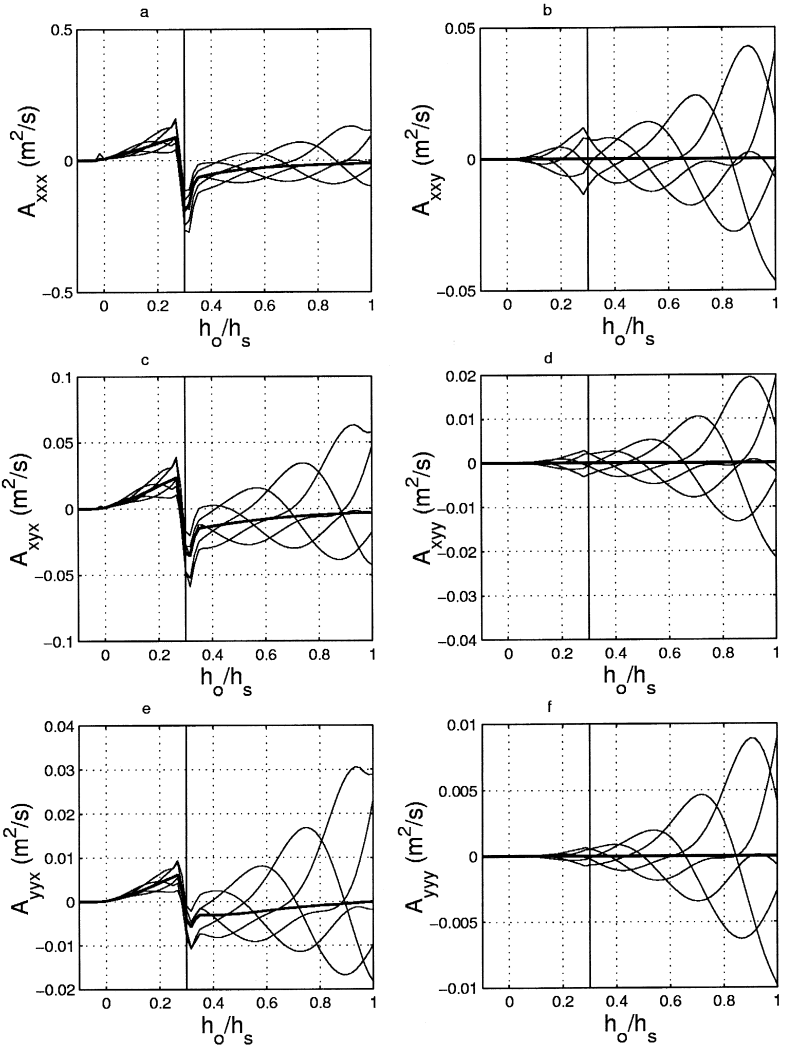

Fig. 13. Magnitude of A coefficients vs. cross-shore distance h_o/h_s for five intervals per IG wave period for the case of $\theta_{i,s} = 22.37°$: (a) A_{xxx}; (b) A_{xxy}; (c) A_{xyx}; (d) A_{xyy}; (e) A_{yyx}; and (f) A_{yyy}. The case of no groupiness is indicated by the thick solid line. The still-water shoreline is located at $h_o/h_s = 0$ and the breakpoint at $h_o/h_s = 0.3$.

and a term for the surface contribution

$$E_{\alpha\beta} = V_{1\alpha}^{(0)}(\bar{\zeta})Q_{w\beta} + V_{1\beta}^{(0)}(\bar{\zeta})Q_{w\alpha} \tag{28}$$

so that

$$M_{\alpha\beta} = C_{\alpha\beta} + E_{\alpha\beta} \tag{29}$$

Fig. 12 shows the dimensional values of $C_{\alpha\beta}$ and $E_{\alpha\beta}$ as defined in Eqs. (27) and (28), respectively. The time variation over the group period is again very significant. As in the previous figure, the C_{xx} and E_{xx} coefficients are larger than the C_{xy} and C_{xy} coefficients, which are in turn larger than the C_{yy} and C_{yy} coefficients, due to the refraction of the wave groups towards the shore-normal.

The E coefficients are of equal magnitude and even slightly larger than the corresponding C coefficients, especially just inside the breakpoint ($h_o/h_s < 0.3$), where the surface velocities become large due to the large gradients in the forcing and the large local value of the short-wave-induced volume flux $Q_{w\beta}$ in the breaking waves. In fact, it will be shown below that the equivalent terms in the equations have a very significant effect.[2]

Finally, Fig. 13 shows the variation of the $A_{\alpha\beta\gamma}$ coefficients. Since this term is symmetrical in the first two indices (as was already seen in Eq. (36), we can reduce the number of A coefficients from eight to six. The figure shows that the A_{xxx} term is much larger than all the other coefficients. It can also be seen that seawards of the breakpoint the values of all these coefficients are larger than in the surf zone. However, in the momentum equations, these coefficients are multiplied by $\tilde{U}$ and $\tilde{V}$, which both tend to zero offshore. As will be shown in the next section, this means that the importance of these terms is relatively small offshore. The values of $A_{\alpha\beta\gamma}$ vary significantly across the breakpoint because they depend on the horizontal gradients of the rapidly changing velocity profiles (see Eq. (36)). This means that, in the governing equations, we can expect some of these A terms to be large around the breakpoint. The contribution of these and all other Q3D terms to the momentum equations will be shown in the next section.

4.4. Analysis of Q3D contributions to the momentum equations

As mentioned the isolated analysis of the Q3D mixing coefficients given in the previous section only gives a partial picture of the mixing effect. To fully assess the importance of the nonlinear processes described by these coefficients, we need to look at the corresponding terms in the equations. The analysis is performed at an arbitrary time after the periodic state of the IG waves has been reached and is strictly speaking only valid for this particular time. However, similar analysis of the variation for other times show that the magnitudes of the terms in the equations at this time instance are indeed characteristic for their magnitudes at any time in the periodic state.

We first analyze the terms in the x-momentum equation for the case of normal incidence (all terms in the y-momentum equation are identically zero). Fig. 14 shows the most important terms in the x-momentum equation. The "conventional" terms shown are the pressure gradient $gh(\partial\zeta/\partial x)$, the radiation stress gradient $(1/\rho)(\partial S_{xx}/\partial x)$

[2] For the short-wave model used here, the variation right around the breakpoint is somewhat exaggerated due to the sudden changes in wave height assumed in that region. However, the conclusion holds also for more realistic variations of the change in wave height at the initiation of breaking.

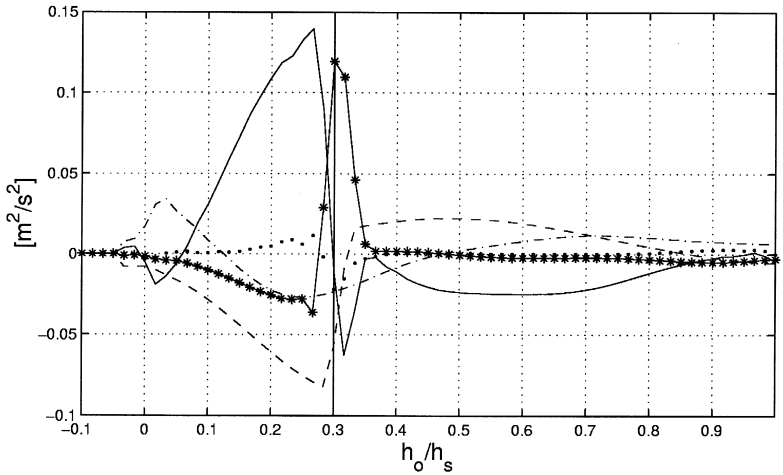

Fig. 14. Magnitude of significant terms in x the momentum equation vs. cross-shore distance h_o / h_s for the case of $\theta_{i,s} = 0°$: pressure gradient (solid); radiation stress gradient $((1/\rho)\partial S_{xx}/\partial x)$ (dashed); local acceleration (dash-dotted); $\partial M_{xx}/\partial x$ (stars); and $(\partial/\partial x)(h(B_{xx} + 2D_{xx} + 2\nu_t)(\partial\tilde{V}/\partial x))$ (dots). The still-water shoreline is located at $h_o / h_s = 0$ and the breakpoint at $h_o / h_s = 0.3$.

and the local acceleration. Of the Q3D terms, the $(\partial M_{xx}/\partial x)$ term is large only locally at the breakpoint. This is due to the choice of a fixed breaker location ($\kappa = 0$), which causes the cross-shore velocity profiles to undergo a rapid change over a short distance around the breakpoint. (Notice that M_{xx} is equivalent to the momentum correction factor in hydraulics.) The term is positive, which leads to a negative pressure gradient in the balance. In the inner surf zone, this term is found comparable to other terms, and is negative, which causes an increase in the pressure gradient and explains the difference between the envelopes of Fig. 5. Also shown is the sum of the B_{xx} and D_{xx} dispersive mixing terms, which has a minor contribution to the cross-shore momentum balance. Hence, we have confirmed that the original result of Svendsen and Putrevu (1994) that the cross-shore momentum balance is only affected to a minor degree by the dispersive mixing can be indeed be extended to 2DH situations.

For the case of obliquely incident wave groups, Fig. 15 shows the most important terms in the x- and y-momentum equations. Fig. 15(a) shows the leading terms in the x-momentum equation, which are the same as in the normal-incidence case.

The dominating terms in the y component of Eq. (10) are shown in Fig. 15(b) and (c). Those terms are (as can be expected) the local acceleration, the pressure gradient $gh(\partial\bar{\zeta}/\partial y)$, the radiation shear stresses $(1/\rho)(\partial S_{xy}/\partial y)$ and $(1/x)(\partial S_{yy}/\partial y)$, the advection term $(\partial/\partial x)(\overline{Q}_x\overline{Q}_y/h)$, and the bottom friction. However, we also see that in the longshore direction, the two Q3D terms, $\partial M_{xy}/\partial x$ and $(\partial/\partial x)(hD_{xx}(\partial\tilde{V}/\partial x))$ are important. The first term is significant around the breakpoint for the same reason that the $\partial M_{xx}/\partial x$ was in the x-momentum equation. The second term is of the same order of magnitude as the 2DH terms inside the surf zone and is the same that was found to be in the dispersion of momentum in the case of a steady longshore current (Svendsen and

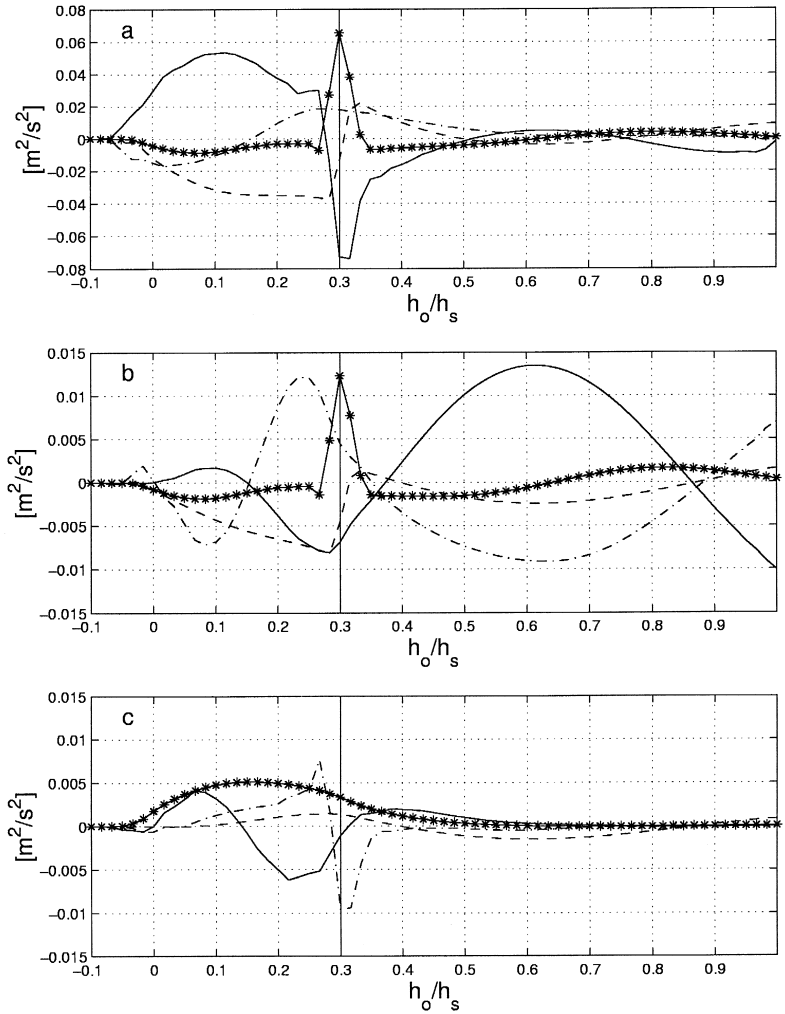

Fig. 15. Magnitude of significant terms in the momentum equations vs. cross-shore distance h_o/h_s. (a) x-Momentum equation: as in the previous figure; (b) y-momentum equation: pressure gradient (solid), radiation stress gradient $(1/\rho)(\partial S_{xy}/\partial x)$ (dashed), local acceleration (dash-dotted) and $\partial M_{xy}/\partial x$ (stars); (c) y-momentum equation: advective acceleration $(\partial/\partial x)(\overline{Q}_x\overline{Q}_y/h)$ (solid), $(1/\rho)(\partial S_{yy}/\partial y)$ (dashed), $-(\partial/\partial x)(hD_{xx}(\partial\tilde{V}/\partial x))$ (dash-dotted) and bottom friction (stars). The still-water shoreline is located at $h_o/h_s = 0$ and the breakpoint at $h_o/h_s = 0.3$.

Putrevu, 1994). In the present case — where the shear in the longshore current is also large — this term is again important. This is in accordance with the observation pointed out by Sancho and Svendsen (1997) that the forcing in longshore direction is usually an order of magnitude smaller than in the cross-shore direction, which implies that the dispersive terms become relatively more important in longshore momentum balance.

This illustrates that while the Q3D coefficients may exhibit a large temporal and spatial variation, their final contribution to the governing equations is controlled by the local IG wave velocity and current shear with which they appear in the momentum equations. In this case of a longshore uniform beach, the $\partial\tilde{V}/\partial x$ shear is significantly larger than the other velocity shears, and only those Q3D coefficients, which are multiplied by this shear have a significant contribution. Releasing the constraint of a longshore-uniform beach, for instance in the case of a barred beach with a rip channel, will allow other velocity shears to become (locally) large so that other Q3D terms become significant as well.

5. Conclusions

A numerical study of the forcing of leaky IG waves by normally and obliquely incident wave groups is performed using the SHORECIRC model which incorporates the Q3D terms generated by the depth variation of the velocity profiles. The governing equations are derived from basic principles and include the effect of the depth variation of the long waves by means of semi-analytical solutions.

The numerical model including the boundary conditions is described briefly. The model's accuracy (in linearized form) is verified by comparing to the analytical solution for the linear surf beat envelope generated by a weakly modulated carrier wave (Schäffer 1993, 1994).

The largest effect of the Q3D terms is in the dispersive mixing effect of the shore-parallel momentum. This effect primarily acts to modify the mean longshore current, which is generated by the carrier wave as described by Svendsen and Putrevu (1994).

However, for the case of normally incident and obliquely incident wave groups, represented as a weakly modulated carrier wave, it is shown that a slight modulation in the wave heights of 10% due to wave groupiness causes large temporal and spatial variations in the Q3D coefficients, relative to the case of no groupiness. The increase in magnitude of the coefficients due to the groupiness is about a factor 2.

It is also shown that only those Q3D coefficients, which appear in combination with the largest velocity shears, make a significant contribution to the momentum equations and are of comparable size relative to the 2DH terms retained in conventional nonlinear shallow water models. The largest 3D terms are the lateral dispersive mixing term and the momentum correction factor.

These Q3D terms turn out to have a significant effect on the structure of the cross-shore envelope of the forced IG waves, especially around the breakpoint and in the inner surf zone. These terms cause a larger cross-shore gradient of the surface elevation in the surf zone.

From the model equations, the vertical IG wave velocity profiles can also be determined. For locations inside the surf zone, these exhibit a large curvature and time variation in the cross-shore direction, and a small — but essential — depth variation in the longshore direction. Outside the surf zone, the velocities in the longshore direction are small, while in the cross-shore direction, only the upper part of the profile is curved.

Acknowledgements

H.A. Schäffer is gratefully acknowledged for providing his analytical IG wave solutions. This work is a result of research sponsored by NOAA Office of Sea Grant, Department of Commerce, under Award No. NA 56 RG 0147 (Project No. R/OE-17) and by the US Army Research Office, University Research Initiative under Contract No. DAAL03-92-G-0116. The first author received additional funding from the Netherlands Centre for Coastal Research (NCK) and Delft University of Technology. The US Government is authorized to produce and distribute reprints for government purposes notwithstanding any copyright notation that may appear herein.

Appendix A. Substitution of the depth-dependent terms by depth-invariant coefficients

The replacement of the depth-dependent terms with depth-invariant coefficients can be achieved by using the local (i.e., not depth-integrated), time-averaged momentum equations (see, e.g., Svendsen and Lorenz, 1989), which after some manipulations can be written as (Van Dongeren and Svendsen, 1997b)

$$\frac{\partial V_{1\beta}}{\partial t} - \frac{\partial}{\partial z}\left(\nu_t \frac{\partial V_{1\beta}}{\partial z}\right) = -\beta_\beta + \frac{1}{\rho h}\frac{\partial}{\partial x_\alpha}\left(S_{\alpha\beta} - \overline{\int_{-h_o}^{\zeta} \tau_{\alpha\beta}\,\mathrm{d}z}\right) - \frac{\tau_\beta^S - \tau_\beta^B}{\rho h} - V_{1\alpha}\frac{\partial \tilde{V}_\beta}{\partial x_\alpha} - \tilde{V}_\alpha \frac{\partial V_{1\beta}}{\partial x_\alpha} - W\frac{\partial V_{1\beta}}{\partial z} \tag{30}$$

where

$$\beta_\beta = \frac{\partial}{\partial x_\alpha}\left(\overline{u_{w\alpha}u_{w\beta}} - \overline{w_w^2}\right) + \frac{\partial \overline{u_{w\beta}w_w}}{\partial z} - \frac{\partial}{\partial x_\alpha}\left(\nu_t\left(\frac{\partial \tilde{V}_\alpha}{\partial x_\beta} + \frac{\partial \tilde{V}_\beta}{\partial x_\alpha}\right)\right) \tag{31}$$

In this expression, w_w denotes the vertical short-wave velocity and ν_t is the turbulent eddy viscosity and we have expressed the turbulent shear stresses as (e.g., Rodi, 1980),

$$\tau_{\alpha\beta} = \rho\nu_t\left(\frac{\partial \tilde{V}_\alpha}{\partial x_\beta} + \frac{\partial \tilde{V}_\beta}{\partial x_\alpha}\right) \tag{32}$$

In Eq. (30), small terms included in the full version of the equation have been omitted. See Putrevu and Svendsen (1999) for a detailed discussion of the expected magnitude of the terms in the full equation.

Eq. (30) can be solved more easily if we split the depth-varying velocity into two parts

$$V_{1\beta} = V_{1\beta}^{(0)} + V_{1\beta}^{(1)} \tag{33}$$

The first part of $V_{1\beta}^{(0)}$ is primarily the (slowly time-varying) component generated by the local external forcing, which are the first five terms on the RHS of Eq. (30), while the second smaller contribution is generated by the advective terms (the last three terms on the RHS) in Eq. (30). Hence, we can solve for $V_{1\beta}^{(0)}$, which represents the first approximation to the depth-varying part of the IG velocity profiles, which is done for the quasi-steady state in Appendix B.

Following the derivation of Putrevu and Svendsen (1997, 1999), which is omitted here for brevity, we can define the coefficients

$$D_{\alpha\gamma} \equiv \frac{1}{h}\int_{-h_o}^{\bar{\zeta}} V_{1\alpha}^{(0)} \int_{z}^{\bar{\zeta}} \frac{1}{\nu_t} \int_{-h_o}^{z} V_{1\gamma}^{(0)} (\mathrm{d}z)^3 \tag{34}$$

$$M_{\alpha\beta} \equiv \int_{-h_o}^{\bar{\zeta}} V_{1\alpha}^{(0)} V_{1\beta}^{(0)} \mathrm{d}z + V_{1\alpha}^{(0)}(\bar{\zeta}) Q_{w\beta} + V_{1\beta}^{(0)}(\bar{\zeta}) Q_{w\alpha} \tag{35}$$

$$\begin{aligned} A_{\alpha\beta\gamma} \equiv & -\int_{-h_o}^{\bar{\zeta}} V_{1\alpha}^{(0)} \int_{z}^{\bar{\zeta}} \frac{1}{\nu_t} \left(\frac{\partial}{\partial x_\gamma} \int_{-h_o}^{z} V_{1\beta}^{(0)} \mathrm{d}z - V_{1\beta}^{(0)} \frac{\partial h_o}{\partial x_\gamma} \right) (\mathrm{d}z)^2 \\ & -\int_{-h_o}^{\bar{\zeta}} V_{1\beta}^{(0)} \int_{z}^{\bar{\zeta}} \frac{1}{\nu_t} \left(\frac{\partial}{\partial x_\gamma} \int_{-h_o}^{z} V_{1\alpha}^{(0)} \mathrm{d}z - V_{1\alpha}^{(0)} \frac{\partial h_o}{\partial x_\gamma} \right) (\mathrm{d}z)^2 \end{aligned} \tag{36}$$

$$\begin{aligned} B_{\alpha\beta} \equiv & \frac{1}{h}\int_{-h_o}^{\bar{\zeta}} V_{1\alpha}^{(0)} \int_{z}^{\bar{\zeta}} \frac{1}{\nu_t} \int_{-h_o}^{z} V_{1\beta}^{(0)} (\mathrm{d}z)^3 - \frac{1}{h}\int_{-h_o}^{\bar{\zeta}} V_{1\alpha}^{(0)} \int_{z}^{\bar{\zeta}} \frac{1}{\nu_t} V_{1\beta}^{(0)} (h_o + z) (\mathrm{d}z)^2 \\ & -\frac{1}{h}\int_{-h_o}^{\bar{\zeta}} V_{1\beta}^{(0)} \int_{z}^{\bar{\zeta}} \frac{1}{\nu_t} V_{1\alpha}^{(0)} (h_o + z) (\mathrm{d}z)^2 \end{aligned} \tag{37}$$

These expressions appear when the solution for $V_{1\alpha}^{(0)}$ is substituted into the depth-dependent integrals in Eq. (8). We get for these integrals

$$\begin{aligned} & \int_{-h_o}^{\bar{\zeta}} V_{1\alpha} V_{1\beta} \mathrm{d}z + \overline{\int_{\zeta_t}^{\zeta} u_{w\alpha} V_{1\beta} + u_{w\beta} V_{1\alpha} \mathrm{d}z} \\ & \quad \approx M_{\alpha\beta} - h\left(D_{\alpha\gamma} \frac{\partial \tilde{V}_\beta}{\partial x_\gamma} + D_{\beta\gamma} \frac{\partial \tilde{V}_\alpha}{\partial x_\gamma} + B_{\alpha\beta} \frac{\partial \tilde{V}_\gamma}{\partial x_\gamma} \right) + A_{\alpha\beta\gamma} \tilde{V}_\gamma \end{aligned} \tag{38}$$

This expression is substituted into Eq. (8) to get the Q3D horizontal momentum equations.

Appendix B. Quasi-steady-state approximation and calculation of the coefficients

If we nondimensionalize the left-hand side of Eq. (30) using

$$t = Tt' \qquad z = h_b z' \qquad \nu_t = C_\nu h_b \sqrt{g h_b}\, \nu_t' \qquad V_{1\beta}^{(0)} = c_b V_{1\beta}'^{(0)} \tag{39}$$

where T is a typical time scale of the long-wave motion, C_ν is a proportionality constant and h_b and c_b are the depth and celerity at breaking, respectively. The nondimensionalized left-hand side of Eq. (30) then becomes

$$\frac{c_b}{T}\frac{\partial V'^{(0)}_{1\beta}}{\partial t} - \frac{C_\nu c_b h_b \sqrt{g h_b}}{h_b^2}\frac{\partial}{\partial z'}\left(\nu'_t \frac{\partial V'^{(0)}_{1\beta}}{\partial z'}\right) \tag{40}$$

This implies that the acceleration is small if the parameter

$$\frac{1}{C_\nu T}\sqrt{\frac{h_b}{g}} \ll 1 \tag{41}$$

Under these assumptions, Eq. (30) reduces to a second-order equation in z and can be solved with two boundary conditions, for which we choose

$$\frac{\partial V^{(0)}_{1\beta}}{\partial z} = \frac{\tau^B_\beta}{\rho \nu_t} \quad \text{at} \quad z = -h_o \tag{42}$$

which assumes a slip velocity and an associated stress, and

$$\int_{-h_o}^{\bar{\zeta}} V^{(0)}_{1\beta} \mathrm{d}z = -Q_{w\beta} \tag{43}$$

If we define

$$f_\beta \equiv \beta_\beta - \frac{1}{\rho h}\frac{\partial}{\partial x_\alpha}\left(S_{\alpha\beta} - \overline{\int_{-h_o}^{\zeta} \tau_{\alpha\beta}\mathrm{d}z}\right) + \frac{\tau^S_\beta - \tau^B_\beta}{\rho h} \tag{44}$$

and integrating Eq. (30) twice for $V^{(0)}_{1\beta}$ while applying the boundary conditions, we get the velocity profile

$$V^{(0)}_{1\beta} = b_1 \xi^2 + b_2 \xi + b_3 \tag{45}$$

where

$$b_1 = \frac{f_\beta}{2\nu_t} \tag{46}$$

$$b_2 = \frac{\tau^B_\beta}{\rho \nu_t} \tag{47}$$

$$b_3 = -\left(\frac{b_1}{3}h^2 + b_2\frac{h}{2} + \frac{Q_{w\beta}}{h}\right) \tag{48}$$

and where the vertical coordinate z has been transformed to a new coordinate ξ, under the transformation $\xi = z + h_o$, which means that $\xi = 0$ at the local bottom and $\xi = h = h_o + \bar{\zeta}$ at the mean surface elevation.

Putrevu and Svendsen (1997, 1999) show that this expression is the first approximation to the time-dependent solution of Eq. (30). Hence, in the quasi-steady approximation, the velocity profiles are quadratic and known so that the Q3D coefficients (Eqs. (34)–(37)) can be expressed in terms of the coefficients of the velocity profiles.

Equivalent to Eq. (45), we can write

$$V_{1\alpha}^{(0)} = a_1 \xi^2 + a_2 \xi + a_3 \tag{49}$$

where a_1, a_2 and a_3 have the equivalent definitions for direction α.

Using Eqs. (45) and (49), we can then express the coefficients, Eqs. (34)–(37), in terms of known variables and parameters. After some manipulations, the dispersion coefficient, Eq. (34), can be rewritten as

$$D_{\alpha\beta} = \frac{1}{\nu_t}\left(a_1 b_1 \frac{h^6}{63} + (a_1 b_2 + a_2 b_1)\frac{h^5}{36} + \left(a_1 b_3 + \frac{3}{4} a_2 b_2 + a_3 b_1\right)\frac{h^4}{15} + (a_2 b_3 + a_3 b_2)\frac{h^3}{8} + a_3 b_3 \frac{h^2}{3}\right) \tag{50}$$

Notice that the result is symmetrical in a and b or, in other words, in direction.

We can write Eq. (35) as

$$M_{\alpha\beta} = a_1 b_1 \frac{h^5}{5} + (a_1 b_2 + a_2 b_1)\frac{h^4}{4} + (a_1 b_3 + a_2 b_2 + a_3 b_1)\frac{h^3}{3} + (a_2 b_3 + a_3 b_2)\frac{h^2}{2} + a_3 b_3 h + \left(a_1 h^2 + a_2 h + a_3\right) Q_{w\beta} + \left(b_1 h^2 + b_2 h + b_3\right) Q_{w\alpha} \tag{51}$$

which is also directionally symmetrical.

Eq. (36) can be expressed as

$$A_{\alpha\beta\gamma} = -\frac{1}{\nu_t}\left[\frac{\partial a_1 b_1}{\partial x_\gamma}\frac{h^7}{63} + \left(\frac{\partial a_1 b_2}{\partial x_\gamma} + \frac{\partial a_2 b_1}{\partial x_\gamma}\right)\frac{h^6}{36} + \left(\frac{\partial a_1 b_3}{\partial x_\gamma} + \frac{\partial a_3 b_1}{\partial x_\gamma}\right)\frac{h^5}{15} + \frac{\partial a_2 b_2}{\partial x_\gamma}\frac{h^5}{20} + \left(\frac{\partial a_2 b_3}{\partial x_\gamma} + \frac{\partial a_3 b_2}{\partial x_\gamma}\right)\frac{h^4}{8} + \frac{\partial a_3 b_3}{\partial x_\gamma}\frac{h^3}{3}\right] \tag{52}$$

This expression is symmetrical in the first two indices.

Finally, Eq. (37) becomes

$$B_{\alpha\beta} = -\frac{h^3}{\nu_t}\left[\frac{4}{63} a_1 b_1 h^3 + (a_1 b_2 + a_2 b_1)\frac{h^2}{12} + a_2 b_2 \frac{h}{10} + \frac{2}{15}(a_1 b_3 + a_3 b_1) h + \frac{1}{8}(a_2 b_3 + a_3 b_2)\right] \tag{53}$$

which is also symmetrical.

References

Chen, Y., 1998a. Resonant scattering of edge waves by longshore periodic topography. J. Fluid Mech. 369, 91–123.

Chen, Y., 1998b. Resonant scattering of edge waves by longshore periodic topography: finite beach slope. J. Fluid Mech. 387, 255–269.

De Vriend, H.J., 1987. Quasi-3D modelling of nearshore currents. Coastal Eng. 11, 565–601.

Ebersole, B., Dalrymple, R.A., 1980. Numerical modeling of nearshore circulation. In: Edge, B.L. (Ed.), Proc. of the 17th International Conference on Coastal Engineering. ASCE, New York, pp. 2710–2725.

Elder, J.W., 1959. The dispersion of marked fluid in turbulent shear flow. J. Fluid Mech. 5, 544–560.

Fisher, H.B., 1978. On the tensor form of the bulk dispersion coefficient in a bounded skewed shear flow. J. Geophys. Res. 83, 2373–2375.

Haas, K.A., Svendsen, I.A., Haller, M.C., 1998. Numerical modelling of nearshore circulation on a barred beach with rip current. In: Edge, B.L. (Ed.), Proc. of the 26th International Conference on Coastal Engineering. ASCE, New York, pp. 801–814.

Haller, M.C., Dalrymple, R.A., 1999. Rip current dynamics and nearshore circulation. Research report CACR-99-05. Center for Applied Coastal Research, University of Delaware, Newark.

Kostense, J.K., 1984. Measurements of surf beat and set-down beneath wave groups. In: Edge, B.L. (Ed.), Proc. of the 19th International Conference on Coastal Engineering. ASCE, New York, pp. 724–740.

Lippmann, T.C., Holman, R.A., Bowen, A.J., 1997. Generation of edge waves in shallow water. J. Geophys. Res. 112 (C4), 8863–8879.

Longuet-Higgins, M.S., 1962. Radiation stress and mass transport in gravity waves with application to 'surf-beats'. J. Fluid Mech. 8, 565–583.

Mei, C.C., 1983. The Applied Dynamics of Ocean Surface Waves. Wiley, New York, 740 pp.

Noda, E.K., Sonu, C.J., Rupert, V.C. Collins, J.I., 1974. Nearshore circulations under sea breeze conditions and wave–current interactions in the surf-zone. Tetra Tech Rep. TC-149-4.

Phillips, O.M., 1977. The Dynamics of the Upper ocean. Cambridge Univ. Press, Cambridge, UK, 336 pp.

Putrevu, U., Svendsen, I.A., 1991. Wave induced nearshore currents: a study of the forcing, mixing and stability characteristics. Research report CACR-91-11, Department of Civil Engineering, University of Delaware, Newark.

Putrevu, U., Svendsen, I.A., 1992. A mixing mechanism in the nearshore region. In: Edge, B.L. (Ed.), Proc. of the 23rd International Conference on Coastal Engineering. ASCE, New York, pp. 2758–2771.

Putrevu, U., 1995. Infragravity velocity profiles in the surf-zone. J. Geophys. Res. 100 (C8), 16131–16142.

Putrevu, U., 1997. Dispersive mixing in the nearshore. Proc. Coastal Dynamics'97, Plymouth, UK. ASCE, New York, pp. 207–216.

Putrevu, U., 1999. Three-dimensional dispersion of momentum in wave-induced nearshore currents. Eur. J. Mech., B: Fluids 18 (3), 409–428.

Rodi, W., 1980. Turbulence models and their application in hydraulics. Int. Assoc. Hydraul. Res.. Delft, The Netherlands, 104 pp.

Sánchez-Arcilla, A., Collado, F., Lemos, C., Rivero, F., 1990. Another quasi-3D model for surf-zone flows. In: Edge, B.L. (Ed.), Proc. of the 22nd International Conference on Coastal Engineering. ASCE, New York, pp. 316–329.

Sánchez-Arcilla, A., Collado, F., Rodriguez, A., 1992. Vertically varying velocity field in Q3D nearshore circulation. In: Edge, B.L. (Ed.), Proc. of the 23rd International Conference on Coastal Engineering. ASCE, New York, pp. 2811–2824.

Sancho, F.E., Svendsen, I.A., 1997. Unsteady nearshore currents on longshore varying topographies. Research report CACR-97-10. Center for Applied Coastal Research, University of Delaware, Newark, 320 pp.

Schäffer, H.A., 1993. Infragravity wave induced by short-wave groups. J. Fluid Mech. 247, 551–588.

Schäffer, H.A., 1994. Edge waves forced by short-wave groups. J. Fluid Mech. 259, 125–148.

Schäffer, H.A., Svendsen, I.A., 1988. Surf beat generation on a mild slope beach. In: Edge, B.L. (Ed.), Proc. of the 21st International Conference on Coastal Engineering. ASCE, New York, pp. 1058–1072.

Smith, J.M., Svendsen, A., 1995. Modelling time- and depth-varying currents at Supertank. Proc. Coastal Dynamics '95, Gdansk, Poland. ASCE, New York, pp. 245–256.

Stive, M.J.F., 1987. Quasi-3D nearshore current modelling: Wave induced secondary currents. Proc. of a Special Conference on Coastal Hydrodynamics. ASCE, Newark, pp. 356–370.

Svendsen, I.A., Hansen, J.B., 1976. The transformation up to breaking of periodic waves on a beach. In: Edge, B.L. (Ed.), Proc. of the 15th International Conference on Coastal Engineering. ASCE, New York, pp. 477–496.

Svendsen, I.A., 1989. Velocities in combined undertow and longshore currents. Coastal Eng. 13, 55–79.

Svendsen, I.A., Putrevu, U., 1990. Nearshore circulation with 3-D profiles. In: Edge, B.L. (Ed.), Proc. of the 22nd International Conference on Coastal Engineering. ASCE, New York, pp. 241–254.

Svendsen, I.A., 1994. Nearshore mixing and dispersion. Proc. R. Soc. London, Ser. A. 445, 1–16.

Svendsen, I.A., Sancho, E., Oltman-Shay, J., Thornton, B., 1997. Modelling nearshore circulation under field conditions. Proc. ASCE Waves'97, Virginia Beach, USA. pp. 765–776.

Symonds, G., Huntley, D.A., Bowen, A.J., 1982. Two dimensional surf-beat: long wave generation by a time-varying break point. J. Geophys. Res. 87 (C1), 492–498.

Taylor, G.I., 1954. The dispersion of matter in a turbulent flow through a pipe. Proc. R. Soc. London, Ser. A 219, 446–468.

Van Dongeren, A.R., Sancho, F.E., Svendsen, I.A., Putrevu, U., 1994. SHORECIRC: a quasi 3-D nearshore model. In: Edge, B.L. (Ed.), Proc. of the 24th International Conference on Coastal Engineering. ASCE, New York, pp. 2741–2754.

Van Dongeren, A.R., Svendsen, I.A., Sancho, F.E., 1995. Application of the Q3d SHORECIRC model to surfbeat. Proc. Coastal Dynamics, Gdynia, Poland. ASCE, New York, pp. 233–244.

Van Dongeren, A.R., 1997a. An absorbing-generating boundary condition for shallow water models. J. Waterw. Port Coastal Ocean Eng. 123 (6), 303–313.

Van Dongeren, A.R., Svendsen, I.A., 1997b. Quasi 3-D modeling of nearshore hydrodynamics. Research report CACR-97-04. Center for Applied Coastal Research, University of Delaware, Newark, 243 pp.

Van Dongeren, A.R., Reniers, A.J.H.M., Thornton, E.B., 2000. Nonlinear modelling of infragravity wave response during DELILAH. In preparation.

Visser, P.J., 1984. A mathematical model of uniform longshore currents and comparison with laboratory data. Commun. Hydraul.. Department of Civil Engineering, Delft University of Technology, Delft, The Netherlands, Report 84-2, 151 pp.

Wind, H.G., 1986. Rip current generation near structures. J. Fluid Mech. 171, 459–476.

Wu, C.-S., Liu, L.-F., 1985. Finite element modeling of nonlinear coastal currents. J. Waterw. Port Coastal Ocean Eng. 111 (2), 417–432.